iScience

CellPress
OPEN ACCESS

Article

Photothermally carbonized natural kelp for hydrovoltaic power generation

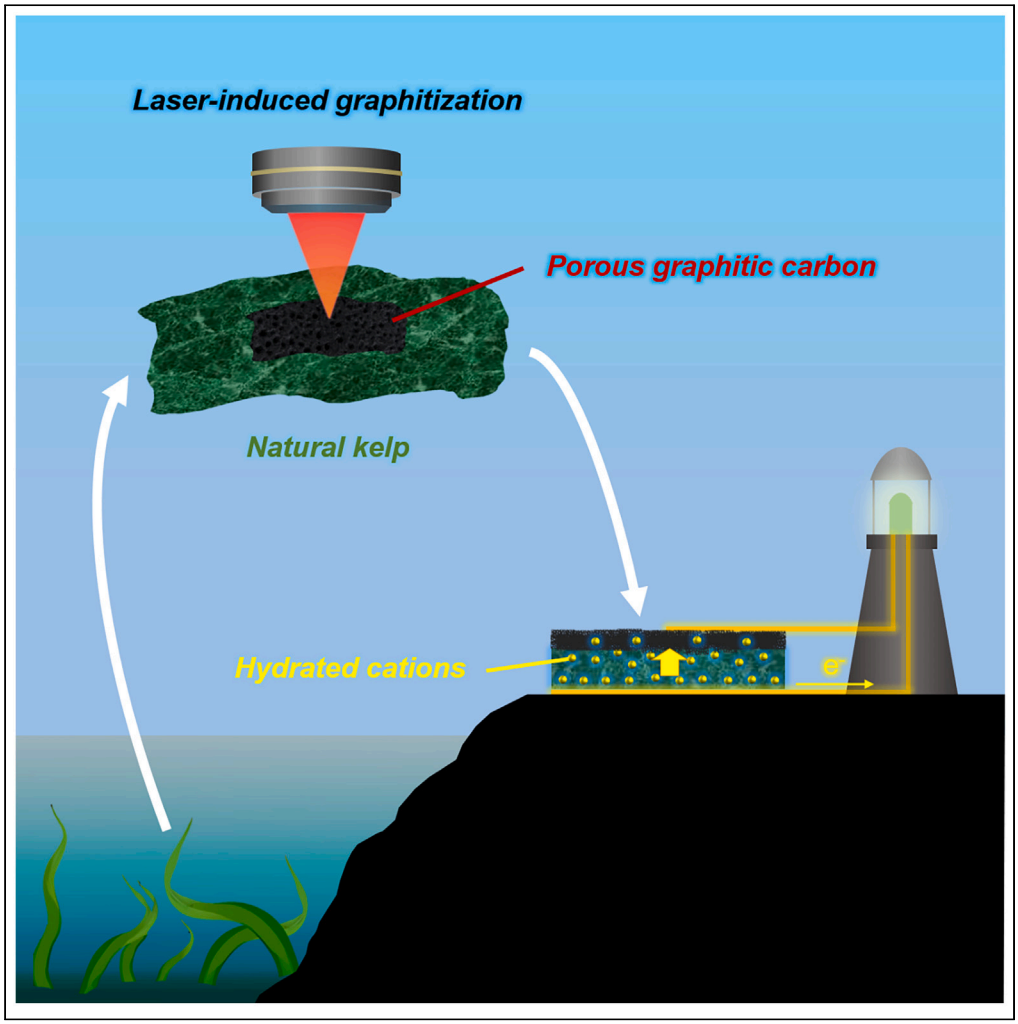

Daewoong Kim, Jakyung Eun, Sangmin Jeon

jeons@postech.ac.kr

Highlights

The hydrovoltaic power generator was developed using photothermally carbonized kelp

Kelp hydrogel functioned as a water reservoir and an ion supplier

The kelp-based HPG generated a voltage of 0.34 V and a current density of 49 μA/cm^2

Kim et al., iScience *27*, 109848
June 21, 2024
https://doi.org/10.1016/j.isci.2024.109848

iScience

CellPress
OPEN ACCESS

Article

Photothermally carbonized natural kelp for hydrovoltaic power generation

Daewoong Kim,[1,2] Jakyung Eun,[1,2] and Sangmin Jeon[1,3,*]

SUMMARY

We have developed an eco-friendly and efficient method for hydrovoltaic power generation through carbonizing natural kelp, a hydrogel with abundant cations. Under ambient conditions, a CO_2 laser beam was focused on the top surface of dried kelp, photothermally converting it into porous graphitic carbon (PGC) and reducing dissociable cations by thermal evaporation. Owing to the preservation of the bottom surface, this photothermal process yielded a PGC–hydrogel membrane (PHM) featuring a cation concentration gradient. With the introduction of deionized water to the intact region, the kelp hydrogel retained a considerable volume of water, creating a moist environment for the PGC. The cation concentration gradient facilitated a continuous migration of cations between the PGC and unaltered kelp, generating a voltage of 0.34 V and a current density of 49 $\mu A/cm^2$. We demonstrated its practical applicability by turning on three light-emitting diodes using an array of eight PHMs.

INTRODUCTION

Hydrovoltaic power generation (HPG), including evaporation-induced power generation and moisture-induced power generation (MPG), has garnered considerable interest as a promising energy harvesting technology owing to its intrinsic benefits such as simplicity, spontaneity, and direct current (DC) outputs.[1–4] In the case of MPG, upon moisture adsorption onto a porous material surface, dissociable species such as oxygen-containing functional groups undergo hydrolysis to produce cations, leading to the migration of the cations along an ion concentration gradient.[5–7] The selective migration of the cations across the negatively charged surface results in charge separation between collecting electrodes and generates a potential difference, creating the flow of electric current through an external circuit.[8–10] Despite the various advantages of MPG, it has a critical disadvantage that its power generation and lifespan significantly degrade under low humidity conditions owing to reduced ion concentration and suppressed ion migration.

To address this limitation, two distinct approaches have been explored. One approach involves the use of hygroscopic materials that can absorb atmospheric moisture effectively even in low humidity conditions,[11,12] while the other approach involves the utilization of liquid water reservoirs. As for the water reservoirs, two alternatives exist: a separate water container (i.e., an external reservoir)[13–15] or an integrated water-containing material such as hydrogel (i.e., an internal reservoir).[16–20] As the utilization of hydrogels simplifies and streamlines the structure of HPG, various hydrogels, such as polyvinyl alcohol (PVA) and polyacrylic acid (PAA) have been utilized in the fabrication of HPGs. Li et al. improved the electrical conductivity of HPG by coating carbon black with a PVA binder on a superabsorbent sponge hydrogel.[16] Yang et al. enhanced water absorption and ion migration using a hydrophilic PVA network crosslinked with phytic acid and glycerin.[18] Liu et al. boosted the ion transport of hydrogel-based HPG by incorporating potassium ions into a PAA-based hydrogel.[21] However, these hydrogel-based HPGs were fabricated by affixing hydrogel to other porous materials.[17,22] Additionally, salts containing monovalent cations were introduced to increase the number of charge carriers, distinct from divalent cations for crosslinking.[23–26]

In this study, we developed a novel HPG by utilizing laser-induced graphitization (LIG) of kelp, a natural hydrogel. Kelp is an ecofriendly material, demonstrating exceptional carbon absorption rates during its growth, which are up to 20 times greater than those observed in terrestrial forests.[27] The kelp hydrogel manifests remarkable water-absorption capabilities and contains abundant minerals, specifically sodium ions that can act as charge carriers. Moreover, the sodium ions enable the conversion of alginate into porous graphitic carbon (PGC) rather than causing ablation during laser irradiation under ambient conditions.[28] By focusing a CO_2 laser beam onto the top surface of dried kelp, the photothermal conversion of the top layer was achieved, resulting in the formation of PGC region with fewer dissociable cations. In contrast, the bottom layer, not in the laser's focus, remains as intact kelp, leading to the formation of a PGC-hydrogel membrane (PHM). Upon introducing water to the intact region, the kelp hydrogel is converted into a water reservoir, thereby promoting sustained water evaporation through the PGC layer. The resulting PHM produced a voltage of 0.34 V and current density of 49 $\mu A/cm^2$ when 30 μL of deionized (DI) water was added onto the bottom surface.

[1]Department of Chemical Engineering, Pohang University of Science and Technology (POSTECH), 77 Cheongam-Ro, Pohang, Gyeongbuk, Republic of Korea
[2]These authors contributed equally
[3]Lead contact
*Correspondence: jeons@postech.ac.kr
https://doi.org/10.1016/j.isci.2024.109848

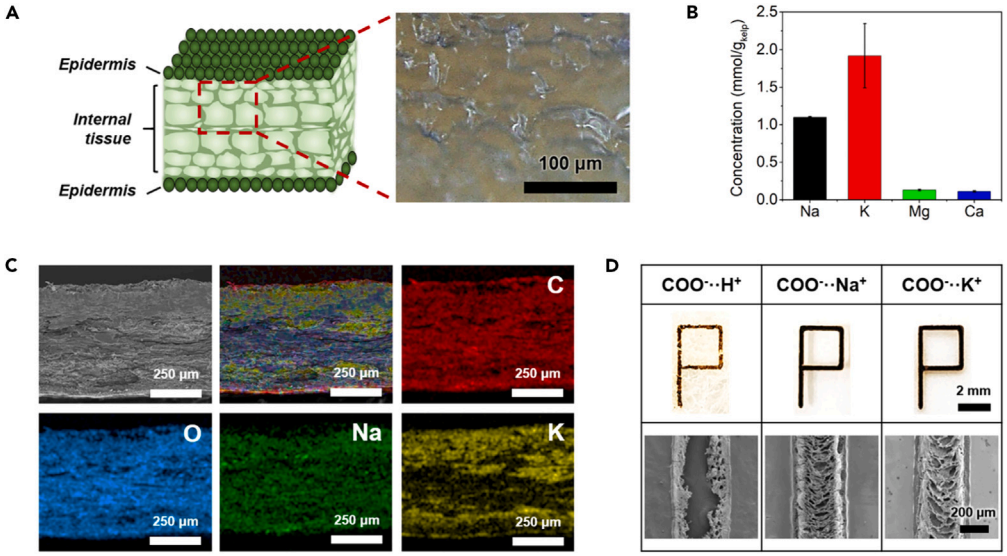

Figure 1. Characterization of the kelp and PGC

(A) Schematic and OM image of cross-sectional microstructure of wet kelp.

(B) Cation concentration in kelp.

(C) Cross-sectional SEM image of dried kelp with an EDS elemental mapping overlay image: carbon (red), oxygen (blue), sodium (green) and potassium (yellow).

(D) OM (upper) and SEM (lower) images of alginate films with varying cations after LIG to shape the letter "P".

RESULTS

Characterization of the kelp and PHM

Figure 1A shows the schematic and OM image of the cross-sectional microstructure of the wet kelp, respectively. The kelp structure comprises epidermal and internal tissues. Chromatophores within the individual epidermal cells impart a brown-green color to the kelp.[29] The cell wall of the internal tissue consists of a microfibrillar skeleton primarily composed of insoluble cellulose and fucoidan, which provides wall rigidity, and an amorphous embedding matrix primarily composed of alginate, which contributes to water absorption.[30] When water is supplied to the internal tissue of the kelp, the apoplast pathway enables efficient water transport through the cell wall,[31] resulting in an internal tissue swelling over 380% of its initial weight (Figure S1). Notably, the water absorption capacity of kelp is comparable to that of superabsorbent materials, with excellent liquid retention even under external pressure. Additionally, marine-cultivated kelp is rich in mineral salts (e.g., KCl and NaCl) that are concentrated within the alginate matrix (Figures 1B and 1C). The cations (Na^+ and K^+) function as charge carriers in HPG and enable the graphitization of alginate instead of ablation during laser irradiation under ambient conditions.[28] Figure 1D shows the OM and enlarged SEM images of alginate films with varying cations (H^+, Na^+ and K^+) after LIG to shape the letter "P" under ambient conditions. The alginate film containing COOH underwent ablation, whereas the ones containing Na^+ or K^+ underwent graphitization. It is worth noting that unlike plant-derived cellulose, which requires additional chemical treatments for flame retardancy, marine-derived kelp possesses inherent flame-retardant properties.

PGC was fabricated by irradiating a CO_2 laser beam on the top surface of the dried kelp. Using a laser power of 3.2 W and a scanning speed of 1 cm/s, the resultant thicknesses measured 130 μm for PGC and 450 μm for the intact kelp. FTIR spectroscopy verified the existence of oxygen-containing functional groups in the kelp and PGC (Figure S2). The broad peak at 3570 cm^{-1} indicates the presence of the hydroxyl groups in both materials.[32] Both kelp and PGC exhibited peaks at 1576 cm^{-1} and 1417 cm^{-1}, corresponding to the asymmetric and symmetric stretching band in the carboxylate group (O-C-O), respectively.[33] A reduction in peak intensities at 2850 cm^{-1} and 2920 cm^{-1}, was observed in PGC, corresponding to -CH_2 stretching vibrations in aliphatic groups.[34] In addition, a new peak appeared at 2350 cm^{-1}, indicative of the conjugated C=C bond,[34] suggesting that graphitization of the kelp occurred during laser irradiation.

Figure 2A shows the cross-sectional SEM image of PHM captured from an oblique angle, with the red dotted box region magnified for closer examination of the PGC–kelp interface. The LIG process of PGC on the kelp substrate is illustrated in Scheme 1A. The porous structure of PGC provides a considerable surface area for increased ion migration and enhanced charge collection at the collector electrode. Given that the laser beam was focused on the top surface, the topmost layer experienced the highest degree of photothermal conversion. The laser intensity diminished along the thickness direction due to being out-of-focus, resulting in the bottommost layer experiencing the lowest degree of photothermal conversion. Given that the focal temperature of the laser beam on the top surface (~2000°C) exceeds the boiling points of NaCl (1465°C) and KCl (1420°C), the mineral particles are vaporized from the top surface of the dried kelp (Figure S3). Owing to the varying laser intensity along the thickness direction, the ratio of the cations (Na^+ and K^+) to carbon at the top surface of PGC (0.08) was lower than that at the PGC–kelp interface (0.27), creating the formation of a high ion concentration gradient in the thickness direction (Table S1). Figures 2B and 2C show the cross-sectional OM images of PGC–kelp before and after the introduction of DI water, respectively. When 30 μL of DI water is

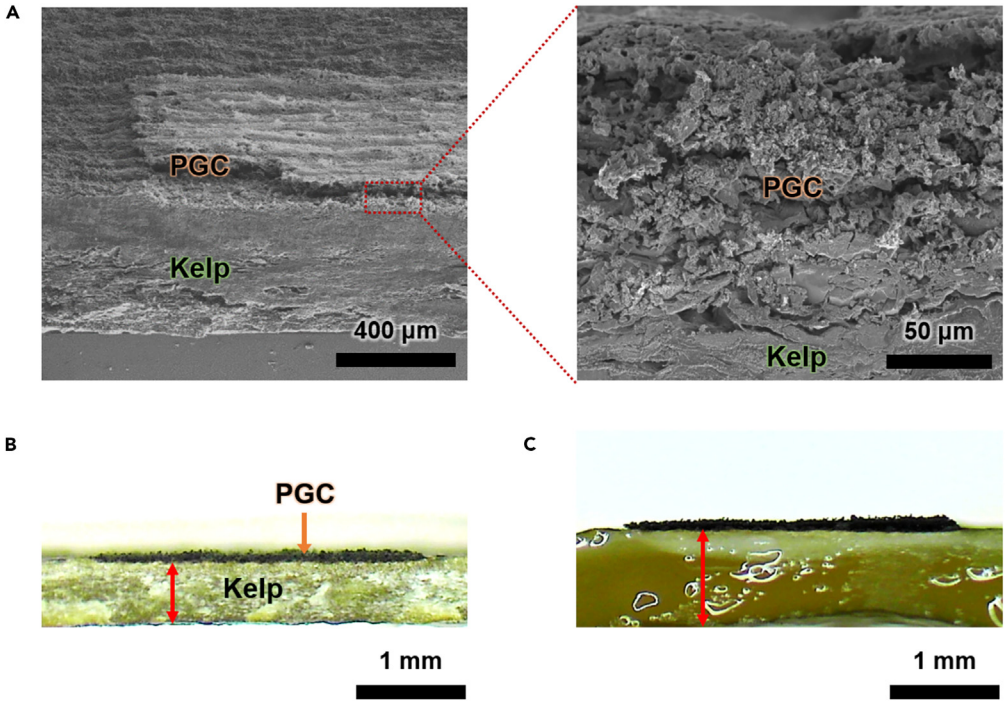

Figure 2. Cross-sectional images of the PHM

(A) Cross-sectional SEM image of PHM captured from an oblique angle (left), including a magnified image of the PGC–kelp interface (right). Cross-sectional OM image of PHM (B) before and (C) after water addition (30 μL). Red arrows indicate the thickness of intact kelp.

applied to the bottom surface (i.e., kelp side), the kelp expands, forming an ~1.0 mm thick hydrogel. This expansion indicates that the kelp hydrogel can function as a water reservoir, allowing the sustained provision of a moist environment in the PGC.

HPG performance of the PHM

To investigate the HPG performance of PHM, water was supplied to its bottom surface using two distinct methods. The structure and optical images of the PHM-based HPG device are shown in Scheme 1B. Figures 3A and 3B show the time-dependent changes in open-circuit voltage and short-circuit current density outputs of PHM, respectively, when DI water was supplied continuously to its bottom surface through a filter paper strip. The voltage output increased as the ions migrated during water evaporation, reaching 0.32 V. Similarly, the current output also increased to 44 μA/cm^2 and remained stable for 10 h, indicating the potential for sustained power generation through continuous water supply. Conversely, when 30 μL of DI water was directly applied onto the bottom surface, the voltage and current outputs attained their maximum values, 0.34 V and 49 μA/cm^2, respectively, and then gradually decreased due to the reduced amount of water in the kelp hydrogel (Figures 3C and 3D). In addition, control experiments demonstrated that the HPG performance of PHM increased with increasing temperature or decreasing RH, due to the facilitated evaporation (Figure S4).

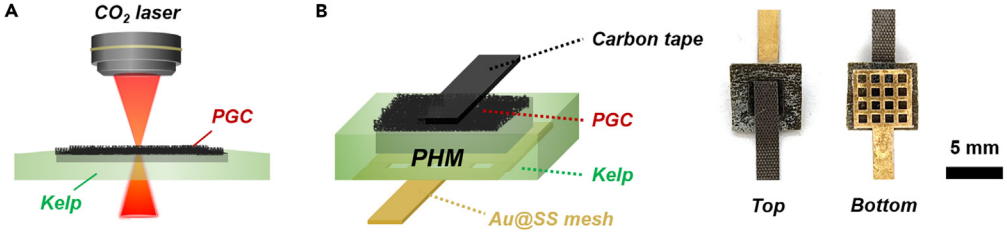

Scheme 1. Schematic and experimental setup of the PHM

(A) Schematic illustration of the fabrication process of PGC on the kelp substrate. CO_2 laser beam focused on the top surface of the kelp, inducing photothermal conversion into PGC, while preserving the bottom surface intact.

(B) Schematic (left) and photos (right) of the PHM-based HPG. Carbon tape was attached to the top surface, while a gold-plated stainless steel mesh was attached to the bottom surface of PHM for current collection.

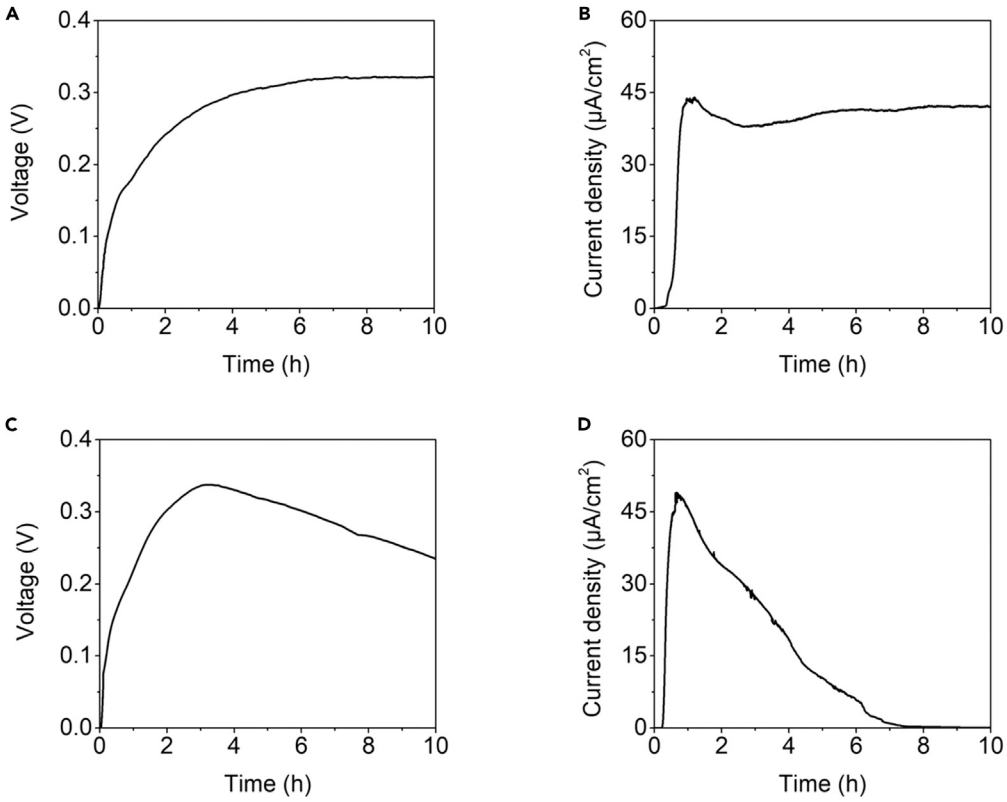

Figure 3. HPG performance of the PHM unit

(A–D) Time-dependent changes in (A) open-circuit voltage and (B) short-circuit current density of PHM when DI water is supplied continuously through a filter paper strip. Time-dependent changes in (C) open-circuit voltage and (D) short-circuit current density of PHM when 30 μL of DI water is directly dropped onto the bottom surface.

Electricity generation mechanism of the PHM-based HPG

Figure 4A illustrates the underlying mechanism of electricity generation in the PHM-based HPG. When water is introduced to the bottom surface of the PHM (i.e., intact kelp), the dry kelp absorbs water, transforming into hydrogel, whereas the PGC layer attains a moist state without absorbing liquid water. To ascertain the non-wettability of the PGC layer, red dye-colored DI water is applied to the bottom surface for 10 h (Figure 4B). A 5 mm × 5 mm white filter paper was positioned atop the PHM to assess whether the dye solution infiltrates the PGC layer, resulting in the wetting of the filter paper. No color change was observed on either surface of the filter paper, after 10 h of water supply, confirming the non-wettability of the PGC layer. Once the kelp layer absorbs water, cations migrate from the kelp layer to the PGC layer due to the ion concentration gradient. The cation (Na^+ and K^+) to carbon concentration ratio at the PGC–kelp interface measures 0.27 (Table S1), which is substantially higher than that at the top surface of PGC (0.08). Note that both the kelp and PGC surfaces carry negative charges, with kelp at −40 mV and PGC at −33 mV, due to the presence of oxygen-containing functional groups like hydroxyl and carboxylate groups (Figure S5). These negative charges facilitate the selective migration of cations, thereby enabling electricity generation. It is noteworthy that the kelp hydrogel without graphitization showed significantly lower voltage and current compared to PHM (Figure S6). This result highlights that the high electrical conductivity and ion concentration gradient of PGC play the key roles in power generation.

To evaluate the influence of carbonization depth on HPG performance, the changes in voltage and current output of the PHM with the depth of carbonization were measured by adjusting the laser scanning speed (Figure S7). When the depth of carbonization is less than 100 μm, the electrical conductivity of the PGC decreases, leading to a significant reduction in current density. However, the HPG performance increases only marginally as the depth of carbonization reaches 200 μm. This is because further carbonization does not significantly enhance electrical conductivity.

A control experiment was conducted to explore the possibility of redox reactions at the electrodes. The CV curves of the PHM-based HPG were compared before and after water supply (Figure S8). Under dry conditions, a linear curve passing through the origin is observed, indicating ohmic behavior. After water supply, the CV curve exhibited capacitive behavior without any peaks associated with redox reactions. This result indicates the absence of electrochemical reactions at the electrode interface, highlighting that electricity generation is achieved through ion migration. To evaluate the influence of the cation content on the performance of the PHM-based HPG, an additional

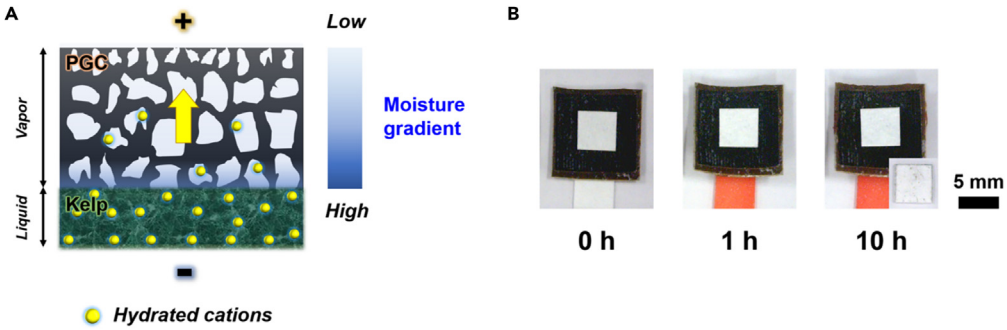

Figure 4. Electricity generation mechanism of the PHM-based HPG

(A) Schematic of electricity generation mechanism of PHM-based HPG.

(B) Time-lapse optical images of a filter paper on PHM as a red dye solution is transported from the bottom surface. 5 mm × 5 mm filter paper was placed on the PHM to determine the non-wettability of the PHM layer. Inset shows the bottom surface of the filter paper, demonstrating that even the bottom surface of the filter paper was not wet by red dye solution after continuous supply for 10 h.

control experiment was performed using kelp that had been rinsed to remove cations. Following an overnight immersion in DI water and subsequent drying, PHM was fabricated from this treated kelp through LIG. The resultant PHM exhibited a reduced voltage of 0.17 V and a current density 6.1 μA/cm^2 under the same conditions, supporting that the hydrated cations played a crucial role as the primary charge carriers (Figure S9).

The current density and maximum power density of PHM were compared with those of hydrogel-based HPGs reported in the literature under similar conditions, specifically those hydrogel-based HPGs that generate continuous outputs through the evaporation of DI water under ambient conditions (Figure S10). The performance of PHM demonstrated higher power outputs due to the rich cation content in kelp. Notably, PHMs are distinct from previous hydrogel-based HPGs that required the inclusion of crosslinking agents.

Application of the PHMs

To demonstrate the practical applicability of PHM as a power generator, it was employed to activate green light-emitting diodes (LEDs). Considering that the onset voltage of a green LED is 2 V, a serial arrangement of eight PHMs was required to attain the necessary voltage output. The open-circuit voltage in Figure 5A exhibits a linear increase, as the number of PHMs connected in series is increased. Figure 5B shows the time-dependent changes in the voltage and current outputs of eight PHMs connected to a 1 MΩ resistor for 30 h. During this period, an additional 30 μL of water was added to the bottom surfaces every 12 h. The voltage and current outputs exhibited an increase upon the addition of 30 μL of water, demonstrating the system's ability to power three LEDs without the need for rectifiers or capacitors. The decreases in the voltage and current outputs are attributed to the decreased amount of water in the hydrogel layer, leading to the reduced rate of ion migration. It is noteworthy that the decreased voltage and current outputs can be restored by introducing an additional 30 μL of water. To further investigate the practical electrical output performance of PHM, it was connected to various external resistors (Figure S11). As the external resistive load ranged from 100 Ω to 100 MΩ, the voltage output increased from 0.0006 V to 0.37 V, whereas the current density decreased from 43 μA/cm^2 to 0.011 μA/cm^2. The maximum power density was 1.88 μW/cm^2 at a resistance of 100 kΩ.

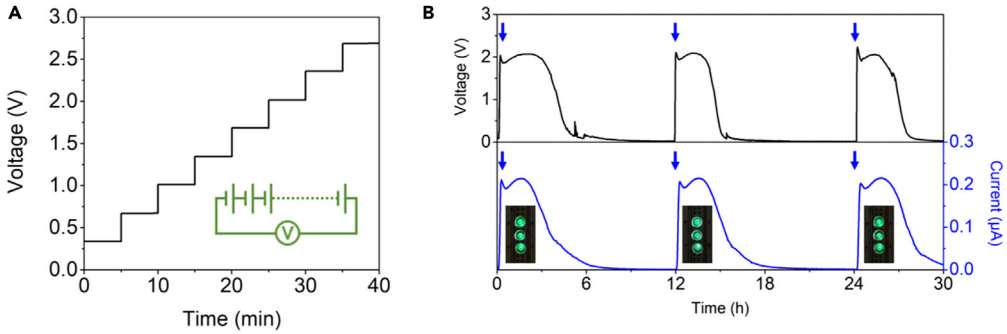

Figure 5. Application of the PHM arrays

(A) Time-dependent changes in open-circuit voltage with the increasing number of PHMs connected in series.

(B) Time-dependent changes in voltage (black) and current (blue) of eight PHMs connected to a 1 MΩ resistor for 48 h. Blue arrows indicate the points at which 30 μL of DI water is dropped onto bottom surface of PHMs. Insets show three green LEDs being powered by eight PHMs in series after water is supplied.

DISCUSSION

We have developed a novel HPG that employs natural kelp as a sustainable and efficient energy source. Through the straightforward irradiation of kelp with an infrared laser under ambient conditions, a PGC forms directly on the surface of the kelp, creating an ion concentration gradient between the PGC and the kelp hydrogel. Furthermore, leveraging the kelp's hydrogel-forming property and high mineral content, the PHM-based HPG sustains a continuous moisture gradient and ion gradient. With the introduction of 30 μL of DI water on the bottom surface, the PHM generates a voltage of 0.34 V and a current density of 49 $\mu A/cm^2$. Notably, the gradual decrease in power output over time can be restored by simply introducing additional water. The PHM-based HPG holds great promise for developing green and efficient power generation systems, utilizing the abundant resources provided by natural kelp.

Limitations of the study

This study presents the innovative use of photothermally carbonized natural kelp for HPG, highlighting its potential in energy harvesting technology. However, the effect of the variations among the natural kelp samples on the consistency of the HPG performance remains uncertain. Although the fabrication cost is expected to remain low due to the inexpensive CO_2 diode laser engraver and the quick irradiation process, further investigation is still required to explore the scalability of natural kelp for practical applications and its economic feasibility.

STAR★METHODS

Detailed methods are provided in the online version of this paper and include the following:

- KEY RESOURCES TABLE
- RESOURCE AVAILABILITY
  - Lead contact
  - Materials availability
  - Data and code availability
- METHOD DETAILS
  - Fabrication of PHM using LIG
  - Instrumental setup for performance evaluation of PHM
- QUANTIFICATION AND STATISTICAL ANALYSIS

SUPPLEMENTAL INFORMATION

Supplemental information can be found online at https://doi.org/10.1016/j.isci.2024.109848.

ACKNOWLEDGMENTS

This work was supported by the National Research Foundation of Korea (NRF) grant funded by the Korea government (MSIT) (No. 2022R1A2C2003234).

AUTHOR CONTRIBUTIONS

D.K. and J.E. contributed equally to this work. D.K. contributed conceptualization, methodology, investigation, validation, visualization, writing – original draft, and writing – review and editing. J.E. contributed conceptualization, methodology, writing – original draft, and writing – review and editing. S.J. contributed conceptualization, supervision, writing – original draft, writing – review and editing, funding acquisition, project administration, and resources.

DECLARATION OF INTERESTS

The authors declare no competing interests.

Received: February 26, 2024
Revised: April 1, 2024
Accepted: April 25, 2024
Published: April 29, 2024

REFERENCES

1. Zhang, Z., Li, X., Yin, J., Xu, Y., Fei, W., Xue, M., Wang, Q., Zhou, J., and Guo, W. (2018). Emerging hydrovoltaic technology. Nat. Nanotechnol. *13*, 1109–1119. https://doi.org/10.1038/s41565-018-0228-6.
2. Dao, V.-D., Vu, N.H., Thi Dang, H.-L., and Yun, S. (2021). Recent advances and challenges for water evaporation-induced electricity toward applications. Nano Energy *85*, 105979. https://doi.org/10.1016/j.nanoen.2021.105979.
3. Yun, T.G., Bae, J., Rothschild, A., and Kim, I.D. (2019). Transpiration Driven Electrokinetic Power Generator. ACS Nano *13*, 12703–12709. https://doi.org/10.1021/acsnano.9b04375.
4. Li, Y., Jiao, S., Dai, Y., Wang, J., Li, J., Kang, N., Irfan, M., and Liu, X. (2023). Spontaneous and sustainable multifunctional transpiration generator for simultaneous harvesting of electricity, freshwater and salt. Appl. Energy *341*, 121110. https://doi.org/10.1016/j.apenergy.2023.121110.
5. Sun, Z., Wen, X., Wang, L., Ji, D., Qin, X., Yu, J., and Ramakrishna, S. (2022). Emerging design principles, materials, and applications for moisture-enabled electric generation. eScience *2*, 32–46. https://doi.org/10.1016/j.esci.2021.12.009.
6. Liu, X., Gao, H., Ward, J.E., Liu, X., Yin, B., Fu, T., Chen, J., Lovley, D.R., and Yao, J. (2020). Power generation from ambient humidity using protein nanowires. Nature *578*, 550–554. https://doi.org/10.1038/s41586-020-2010-9.
7. Zheng, H., Zhou, A., Li, Y., Chen, X., Chen, Y., Xu, Y., Li, Y., Ge, H., and Ning, X. (2023). A sandwich-like flexible nanofiber device boosts moisture induced electricity generation for power supply and multiple sensing applications. Nano Energy *113*, 108529. https://doi.org/10.1016/j.nanoen.2023.108529.
8. Huang, Y., Cheng, H., and Qu, L. (2021). Emerging Materials for Water-Enabled Electricity Generation. ACS Mater. Lett. *3*, 193–209. https://doi.org/10.1021/acsmaterialslett.0c00474.
9. Yan, H., Liu, Z., and Qi, R. (2022). A review of humidity gradient-based power generator: Devices, materials and mechanisms. Nano Energy *101*, 107591. https://doi.org/10.1016/j.nanoen.2022.107591.
10. Shao, B., Song, Y., Song, Z., Wang, Y., Wang, Y., Liu, R., and Sun, B. (2023). Electricity Generation from Phase Transitions between Liquid and Gaseous Water. Adv. Energy Mater. *13*, 2204091. https://doi.org/10.1002/aenm.202204091.
11. Tan, J., Fang, S., Zhang, Z., Yin, J., Li, L., Wang, X., and Guo, W. (2022). Self-sustained electricity generator driven by the compatible integration of ambient moisture adsorption and evaporation. Nat. Commun. *13*, 3643. https://doi.org/10.1038/s41467-022-31221-7.
12. Li, Y., Cui, J., Shen, H., Liu, C., Wu, P., Qian, Z., Duan, Y., and Liu, D. (2022). Useful spontaneous hygroelectricity from ambient air by ionic wood. Nano Energy *96*, 107065. https://doi.org/10.1016/j.nanoen.2022.107065.
13. Liu, X., Ueki, T., Gao, H., Woodard, T.L., Nevin, K.P., Fu, T., Fu, S., Sun, L., Lovley, D.R., and Yao, J. (2022). Microbial biofilms for electricity generation from water evaporation and power to wearables. Nat. Commun. *13*, 4369. https://doi.org/10.1038/s41467-022-32105-6.
14. Garemark, J., Ram, F., Liu, L., Sapouna, I., Cortes Ruiz, M.F., Larsson, P.T., and Li, Y. (2022). Advancing Hydrovoltaic Energy Harvesting from Wood through Cell Wall Nanoengineering. Adv. Funct. Mater. *33*, 2208933. https://doi.org/10.1002/adfm.202208933.
15. Shao, C., Ji, B., Xu, T., Gao, J., Gao, X., Xiao, Y., Zhao, Y., Chen, N., Jiang, L., and Qu, L. (2019). Large-Scale Production of Flexible, High-Voltage Hydroelectric Films Based on Solid Oxides. ACS Appl. Mater. Interfaces *11*, 30927–30935. https://doi.org/10.1021/acsami.9b09582.
16. Li, L., Hao, M., Yang, X., Sun, F., Bai, Y., Ding, H., Wang, S., and Zhang, T. (2020). Sustainable and flexible hydrovoltaic power generator for wearable sensing electronics. Nano Energy *72*, 104663. https://doi.org/10.1016/j.nanoen.2020.104663.
17. Zhao, K., Lee, J.W., Yu, Z.G., Jiang, W., Oh, J.W., Kim, G., Han, H., Kim, Y., Lee, K., Lee, S., et al. (2023). Humidity-Tolerant Moisture-Driven Energy Generator with MXene Aerogel-Organohydrogel Bilayer. ACS Nano *17*, 5472–5485. https://doi.org/10.1021/acsnano.2c10747.
18. Yang, S., Tao, X., Chen, W., Mao, J., Luo, H., Lin, S., Zhang, L., and Hao, J. (2022). Ionic Hydrogel for Efficient and Scalable Moisture-Electric Generation. Adv. Mater. *34*, e2200693. https://doi.org/10.1002/adma.202200693.
19. Zhang, Y., Guo, S., Yu, Z.G., Qu, H., Sun, W., Yang, J., Suresh, L., Zhang, X., Koh, J.J., and Tan, S.C. (2022). An Asymmetric Hygroscopic Structure for Moisture-Driven Hygro-Ionic Electricity Generation and Storage. Adv. Mater. *34*, e2201228. https://doi.org/10.1002/adma.202201228.
20. Liu, C., Wang, S., Wang, X., Mao, J., Chen, Y., Fang, N.X., and Feng, S.-P. (2022). Hydrovoltaic energy harvesting from moisture flow using an ionic polymer–hydrogel–carbon composite. Energy Environ. Sci. *15*, 2489–2498. https://doi.org/10.1039/d2ee00030j.
21. Liu, S., Yang, R., Yang, T., Luo, Z., Su, B., and Lin, X. (2022). Spontaneous energy generation at the air–hydrogel interface with ultrahigh ion activity. J. Mater. Chem. A Mater. *10*, 20905–20913. https://doi.org/10.1039/d2ta05221k.
22. Xu, C., Fu, C., Jiang, Z., Yang, T., and Xin, M. (2023). Hygroelectric Generator Based on Antisymmetric Modification of Graphene Spheres with Ionic Hydrogels. ACS Appl. Nano Mater. *6*, 5930–5938. https://doi.org/10.1021/acsanm.3c00314.
23. Zhang, Y., MohebbiPour, A., Mao, J., Mao, J., and Ni, Y. (2021). Lignin reinforced hydrogels with multi-functional sensing and moist-electric generating applications. Int. J. Biol. Macromol. *193*, 941–947. https://doi.org/10.1016/j.ijbiomac.2021.10.159.
24. Zhang, H., He, N., Wang, B., Ding, B., Jiang, B., Tang, D., and Li, L. (2023). High-Performance, Highly Stretchable, Flexible Moist-Electric Generators via Molecular Engineering of Hydrogels. Adv. Mater. *35*, e2300398. https://doi.org/10.1002/adma.202300398.
25. Zhang, J., Zhuang, J., Lei, L., and Hou, Y. (2023). Rapid preparation of a self-adhesive PAA ionic hydrogel using lignin sulfonate–Al^{3+} composite systems for flexible moisture-electric generators. J. Mater. Chem. A Mater. *11*, 3546–3555. https://doi.org/10.1039/d2ta09687k.
26. He, N., Wang, H., Li, F., Jiang, B., Tang, D., and Li, L. (2023). Ion engines in hydrogels boosting hydrovoltaic electricity generation. Energy Environ. Sci. *16*, 2494–2504. https://doi.org/10.1039/d2ee03621e.
27. Hori, M., Bayne, C.J., and Kuwae, T. (2019). Blue Carbon: Characteristics of the Ocean's Sequestration and Storage Ability of Carbon Dioxide. In Blue Carbon in Shallow Coastal Ecosystems, pp. 1–31. https://doi.org/10.1007/978-981-13-1295-3_1.
28. Lee, S., and Jeon, S. (2018). Laser-Induced Graphitization of Cellulose Nanofiber Substrates under Ambient Conditions. ACS Sustain. Chem. Eng. *7*, 2270–2275. https://doi.org/10.1021/acssuschemeng.8b04955.
29. Shi, N., Li, X., Fan, T., Zhou, H., Ding, J., Zhang, D., and Zhu, H. (2011). Biogenic N-I-codoped TiO_2 photocatalyst derived from kelp for efficient dye degradation. Energy Environ. Sci. *4*, 172–180. https://doi.org/10.1039/c0ee00363h.
30. Davis, T.A., Volesky, B., and Mucci, A. (2003). A review of the biochemistry of heavy metal biosorption by brown algae. Water Res. *37*, 4311–4330. https://doi.org/10.1016/S0043-1354(03)00293-8.
31. Buckley, T.N. (2015). The contributions of apoplastic, symplastic and gas phase pathways for water transport outside the bundle sheath in leaves. Plant Cell Environ. *38*, 7–22. https://doi.org/10.1111/pce.12372.
32. He, Q., Wang, Q., Zhou, H., Ren, D., He, Y., Cong, H., and Wu, L. (2018). Highly crystalline cellulose from brown seaweed Saccharina japonica: isolation, characterization and microcrystallization. Cellulose *25*, 5523–5533. https://doi.org/10.1007/s10570-018-1966-1.
33. Voo, W.-P., Lee, B.-B., Idris, A., Islam, A., Tey, B.-T., and Chan, E.-S. (2015). Production of ultra-high concentration calcium alginate beads with prolonged dissolution profile. RSC Adv. *5*, 36687–36695. https://doi.org/10.1039/c5ra03862f.
34. Mecozzi, M., Pietroletti, M., Scarpiniti, M., Acquistucci, R., and Conti, M.E. (2012). Monitoring of marine mucilage formation in Italian seas investigated by infrared spectroscopy and independent component analysis. Environ. Monit. Assess. *184*, 6025–6036. https://doi.org/10.1007/s10661-011-2400-4.

STAR★METHODS

KEY RESOURCES TABLE

REAGENT or RESOURCE	SOURCE	IDENTIFIER
Chemicals, peptides, and recombinant proteins		
Sodium alginate	Junsei	13035-1201; CAS: 9005-38-3
Hydrochloric acid	Samchun	H0255; CAS: 7647-01-0
Potassium chloride	Sigma-Aldrich	P3911; CAS: 7447-40-7
Other		
Kelp (thickness: 0.5 mm–0.7 mm)	Wando Sea	*Saccharina japonica*
Deionized water system	Human Science	Human Power I^{+}
Carbon tape	LKLabKorea	EST12100
Gold-plated stainless-steel mesh	M-flex	N/A
Filter paper	Advantec	Grade 1
Multimeter	Agilent Technologies	34401A
Sourcemeter	Keithley Instruments	2636B
Scanning electron microscope	JEOL	JSM-7800F

RESOURCE AVAILABILITY

Lead contact

Further information and requests for resources should be directed to and will be fulfilled by the lead contact, Sangmin Jeon (jeons@postech.ac.kr).

Materials availability

This study did not generate new unique reagents.

Data and code availability

This study did not generate any datasets.

- All data reported in this paper will be shared by the lead contact upon request.
- This paper does not report original code.
- Any additional information required to reanalyze the data reported in this paper is available from the lead contact upon request.

METHOD DETAILS

Fabrication of PHM using LIG

A computer-controlled CO_2 laser (wavelength: 10.6 μm) was used to directly convert the top surface of dried kelp into PGC via photothermal conversion. The laser performed line-by-line scans with a spacing of 200 μm, operating at a power level of 3.2 W and a speed of 1 cm/s to form a 3 mm × 3 mm PGC on a 6 mm × 6 mm kelp substrate. As illustrated in Scheme 1A, the laser beam was focused on the top surface of the kelp, with its intensity gradually diminishing toward the bottom surface. This led to the conversion of the top surface into PGC while preserving the original kelp structure on the bottom surface, yielding a PHM. The cation concentration in the kelp was measured using ion chromatography (Thermo Scientific, Dionex, USA). Fourier transform infrared (FTIR) spectrometry (FT/IR-4600, JASCO, Japan) was employed to analyze the functional groups present in the kelp and PGC. The zeta potentials of the kelp and PGC, when dispersed in DI water, were measured using a Zetasizer Nano ZS (Malvern Instruments), respectively. To prepare alginate solutions with varying cations, the COONa groups in sodium alginate dispersions (1 wt. %) were substituted to either COOH or COOK through treatment with 0.1 M HCl or KCl for 1 h, respectively. The resulting solutions were centrifuged to remove the supernatant, which was used to prepare transparent alginate films by drying the solutions under ambient conditions.

Instrumental setup for performance evaluation of PHM

Scheme 1B shows the structure and optical images of the PHM-based HPG device. A carbon tape with a width of 2 mm was affixed to the top surface to function as a charge collector. Concurrently, gold-plated stainless steel mesh electrode was connected to the bottom surface to

construct a PHM-based HPG. The carbon tape electrode was utilized to enable series connection for the formation of multiple PHMs, while the metal mesh electrode was employed to provide mechanical rigidity. To ensure effective electrical contact between the PHM and the electrodes, both sides were pressed using acrylic plates and non-conductive clips. The voltage and current outputs of the PHM-based HPG were measured under ambient conditions (25°C, 50% RH) using a 34401A Multimeter (Agilent Technologies, Santa Clara, CA) and a 2636B SourceMeter (Keithley Instruments, Cleveland, OH), respectively. To investigate the occurrence of electrochemical reactions in the electrodes, cyclic voltammetry (CV) measurements were conducted using CompactStat (Ivium technologies, Netherlands). The morphological features and elemental compositions of PHM were assessed using an optical microscope (BX53, Olympus) and a scanning electron microscope with energy-dispersive X-ray spectroscopy (SEM-EDS, JSM-7800F PRIME, JEOL). To observe the water absorption process of PHM, time-lapse optical images were captured using a hand-held digital microscope (Dino-Lite Premier AM3113T, AnMo Electronics Corporation).

QUANTIFICATION AND STATISTICAL ANALYSIS

The error bars in Figures S1 and S6 represent the standard deviation (SD) obtained using three independent measurements.